Available online at www.sciencedirect.com
SCIENCE DIRECT®
Journal of Physics and Chemistry of Solids 66 (2005) 546–550
JOURNAL OF PHYSICS AND CHEMISTRY OF SOLIDS
www.elsevier.com/locate/jpcs

Unusual properties and reactivity at the nanoscale

James L. Gole[a,b,*], Clemens Burda[a,b], Z.L. Wang[a,b], Mark White[a,b]

[a]Schools of Physics, Material Science and Engineering, and Chemical Engineering, Georgia Institute of Technology, Atlanta, GA 30332-0430, USA
[b]Department of Chemistry, Case Western Reserve University, Cleveland, OH 44106, USA

Accepted 19 June 2004

Abstract

Ready transformation and reactivity is observed at the nanoscale. Silica/silicon (SiO_x) nanospheres of diameter ≤ 30 nm generated from equimolar Si/SiO_2 mixtures are found to display enhanced catalytic and reactive properties relative to commonly employed silica support surfaces including fumed silica. A unique oxygen deficient synthesis has been used to generate SnO_{2-x} nanowires, nanoribbons, and nanotubes displaying the phase coalescence of both ground state rutile and orthohombic structures at pressures well below 0.5 bar. This is in contrast to the bulk where 150 kbar of pressure must be used to generate the orthohombic structure. This unique reactivity and ready transformation is found to accompany the facile (seconds) room temperature nitridation of TiO_2 nanocolloids, efficiently producing photocatalytically active $TiO_{2-x}N_x$ nanoparticles absorbing light well into the visible region. In distinct contrast the direct nitridation of TiO_2 submicron particles does not produce the conversion to the oxynitride at room temperature.

An exciting aspect of research at the nanoscale results as nanostructures hold the potential to display an enhanced and unexpected reactivity relative to that at the micron scale and bulk phase. Further, their formation and interaction may be accompanied by phase transformations not commonly observed in bulk systems. Here, we outline two simple approaches to generate select nanostructures, which are characterized by these distinguishing attributes. We have used a modified-flow tube furnace configuration carefully calibrated for temperature, temperature gradients, entrainment gas flow rate, and total pressure, and variable Si/SiO_2 mixtures to generate silica (SiO_x) nanospheres [1,2] which are found to display enhanced catalytic [3] activity and unexpected reactivity [4]. These structures can be agglomerated to wire-like configurations subsequently providing a means to grow silica nanotubes [2]. Also within this configuration, we have used layered Sn/SnO mixtures to generate SnO_x nanostructures which, at pressures of a few hundred Torr, readily display a phase coexistence between rutile and orthohombic crystal structures [5] normally observed at pressures in excess of 150 kbar in the bulk. The efficacy of these processes at the nanoscale has suggested the application of a highly efficient nitriding process [6] to produce $TiO_{2-x}N_x$ nanoparticles which, in distinction from TiO_2, present highly photocatalytically active quantum dots absorbing light well into the visible region.

Fig. 1 corresponds to an exemplary TEM micrograph of dispersed silica (SiO_x) nanospheres of diameter—30 nm generated in gram quantities on a cold plate placed in the gas flow field of our high temperature synthesis source. Nearly monodisperse particle size distributions for a given experimental run can center on a size between 45 and 8 nm. TEM [1,2], X-ray diffraction [1,2] and ESR [7] measurements demonstrate that the silica nanospheres are amorphous and absent of dangling bonds and defect sites. More recent studies suggest, however, that it will be possible to modify the stoichiometry of these structures from $SiO_x(x>1)$ to $Si_xO(x\geq 2)$ with a judicious choice of experimental conditions. This may, of course, influence defect structure, unpaired electron density, and crystallinity.

The silica nanospheres (Fig. 1) display some surface properties similar to fumed silica produced by the flame hydrolysis of $SiCl_4$ (Cab–O–Sil) albeit in the absence of

* Corresponding author. Address: Schools of Physics, Material Science and Engineering, and Chemical Engineering, Georgia Institute of Technology, Atlanta, GA 30332-0430, USA. Tel.: +1 404 894 4029; fax: +1 404 894 9958.
E-mail address: jim.gole@physics.gatech.edu (J.L. Gole).

0022-3697/$ - see front matter © 2004 Elsevier Ltd. All rights reserved.
doi:10.1016/j.jpcs.2004.06.047

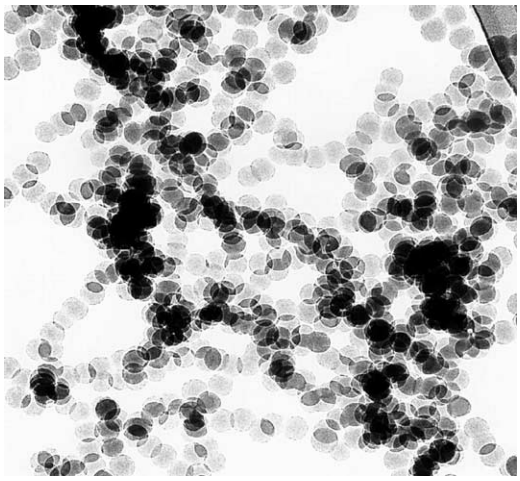

Fig. 1. TEM of virtually 'monodisperse' SiO_2 nanospheres, 30 nm in diameter, synthesized by gas phase condensation from Si/SiO_2.

HCl. They possess silanol groups and have been used as a support for a well-dispersed copper oxide catalyst (formed using the interaction of $Cu(acac)_2$ with the surface silanol groups) and for the selective conversion of ethanol to acetaldehyde [3] in a process at least three times more efficient than that using fumed silica.

Heterogeneous catalysts, adsorbents, and solid state electronic sensors are derived from either single or multiple metal or metalloid oxides [8]. Their surface oxidation states, obtained usually by a post synthesis treatment, determine, at least in part, their performance [9]. However, we have found that by varying the starting material metalloid/oxide ratio it is possible to prepare highly active SiO_x nanospheres with a desired average surface oxidation state without a post synthesis treatment [4]. The surprisingly facile surface chemistry of these structures versus fumed silica has been evaluated using X-ray photoelectron spectroscopy and the phenol hydroxylation reaction in excess hydrogen peroxide. XPS data reveal a distinctly different Si 2p binding energy, 103.15 eV, for the silica nanospheres (Fig. 1) and Cab–O–Sil, 100.35 eV [4]. When these BE's [10] are compared to the literature values for annealed tetravalent [11], 103.4 eV, and zero valent [11], 99.3–99.9, silicon and the non-equilibrium intermediate oxidation states [12] (transition region between Si and SiO_2), +1 (100.5–100.9), and +3 (~103 eV) of surface oxide films [13–16], we are lead to believe that the silicon nanospheres may represent a highly reproducible collection of non-equilibrium phases of silicon and oxygen. The combination of XPS data suggests that the silicon nanospheres (Fig. 1) show an average silicon oxidation state near +3 and, surprisingly, that the Cab–O–Sil sample shows an average oxidation state perhaps as low as +1. These average Si oxidation states may arise from a mixture of 0–4 valency in the regions probed by XPS, however, it is established that the regions below and including the top surface layer have been examined [17]. By comparison, we should also note that the oxidation state of SiO corresponds to divalent silicon, certainly intermediate to the +1 and +3 non-equilibrium states. While SiO might play a role, EDAX data taken for the nanospheres suggest that x is close to 2, consistent also with their measured binding energy.

Table 1
Phenol hydroxylation activity

Absorbent	Rate constant (K, μmol/g h)
Blank	0.02
Cab–O–Sil	0.56
SnO_x/nanospheres	1.41
SiO_x/nanowires	1.70[a]
SiO_x/nanospheres(1)	4.37[a]
SiO_x/nanospheres(2)	4.87[a]

[a] Relative rate constants are closely consistent surface/volume ratio [4,10].

The silicon nanospheres depicted in Fig. 1, generated from an equimolar Si/SiO_2 mix, are considerably more reactive than Cab–O–Sil towards the phenol hydroxylation reaction. This reaction is particularly useful for identifying acid sites [18] and surface oxidation states [19]. The rate constants determined for phenol disappearance given in Table 1, demonstrate that the nanospheres are a factor of eight times more active. While the relative reactivity of silica nanospheres and nanowires generated under similar conditions appears to closely correlate with their surface-to-volume ratio, this is not the case upon comparison with Cab–O–Sil. However, if the silica nanospheres are produced from a mixture of $Si^{4+}(SiO_2)/Si^0 = 0.25$, they show a lower reactivity comparable to Cab–O–Sil for which XPS indicates a surface oxidation state close to +1 as opposed to +4. These results suggest [4,10] that the silicon surface oxidation state as well as the number of surface silanol groups play important roles in determining the activity of these silicon based solids toward the phenol hydroxylation reaction and that the average surface oxidation state can and must be adjusted to promote reaction. At the nanoscale, with its limited particle dimension relative to the bulk, this adjustment may be more easily accomplished. Further, using the outlined approach, the metalloid oxides are prepared in a two-step generalizable process in the absence of liquid solvents, thus offering a more efficient, environmentally friendly, alternate means of adsorbent and catalyst preparation.

With some modification, we have also successfully grown nanowires, sandwiched nanoribbons, and nanotubes of SnO_2 using a layered Sn/SnO source configuration [5]. Here, we find that the chemical composition of these as-synthesized nanostructures can be tuned by introducing oxygen deficiency. We have induced a phase coexistence as the normal rutile structured SnO_2 is accompanied by an orthohombic superlattice structure (Fig. 2). The orientation relationship between orthorhombic SnO_2 and rutile structured SnO_2 is determined to be $[001]_o \| [102]_t$ and $(100)_o \| (010)_t$ for the nanowires and sandwiched

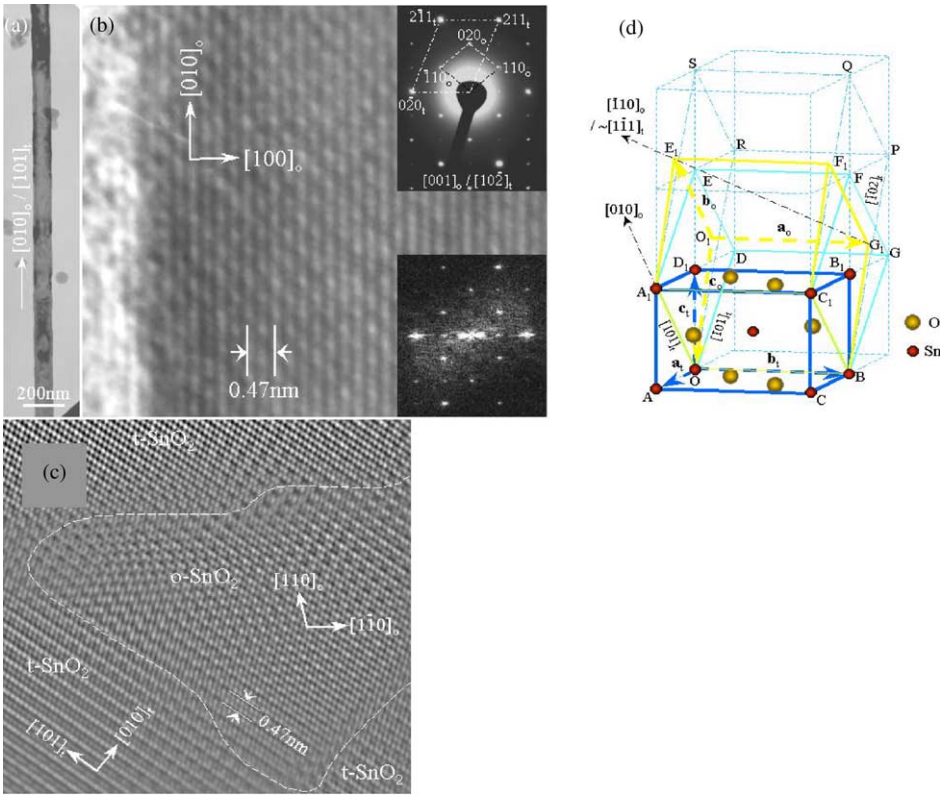

Fig. 2. Low magnification TEM image of an individual orthorhombic SnO_2 nanowire, and (b) the corresponding HRTEM image. The inset at the upper right-hand corner is a select area electron diffraction pattern obtained for the nanowire shown in (a) and the inset at the bottom right-hand corner is a FET of the HRTEM image. (c) HRTEM image showing the domains formed by rutile-SnO_2 and orthorhombic-SnO_2 in the nanoribbons. (d) A schematic diagram of the crystal structures of rutile SnO_2 and orthorhombic SnO_2 where the a_t, b_t, and c_t represent the base vectors of the rutile structured SnO_2, and the a_0, b_0, and c_0 denote the base vectors for the orthorhombic SnO_2.

nanoribbons, and $[001]_o \| [317]_t$ and $(110)_o \| (451)_t$ the nanotubes. While the growth direction of the rutile structured SnO_2 nanowires is along $[101]_t$, two growth directions are found to occur in the nanostructures having the orthohombic SnO_2 structure. They are $[010]_o$ for nanowires and $[110]_o$ for the sandwiched nanoribbons and nanotubes. The orthohombic structure can form in a thin nanowire, co-exist with the normal rutile structured SnO_2 in a sandwiched nanoribbon, or occur in the form of nanotubes. This is a rather surprising result because orthohombic SnO_2 in the bulk can only exist at pressures higher than 150 kbar [20], whereas in the nanostructures it can exist at normal atmospheric pressure. This recently discovered structural characteristic provides a powerful approach for tuning the physical and chemical properties of functional oxides and demonstrates that small is different [21].

There has been a long, continued, interest in TiO_2 based photocatalysis [22] because of the relatively high reactivity and chemical stability of the oxide under UV light excitation ($\lambda < 387$ nm) where this energy exceeds the bandgap of anatase (3.2 eV) crystalline n-TiO_2. However, anatase TiO_2 is a poor absorber in the visible region. The cost and accessibility of UV photons make it desirable to develop photocatalysts which are highly reactive under visible light excitation utilizing the solar spectrum or even interior room lighting.

Recently, Asahi et al. [23] have prepared $TiO_{2-x}N_x$ films by (1) sputtering TiO_2 targets in an N_2 (40%)/Ar gas mixture and then annealing in N_2 gas at 550 °C for 4 h and (2) treating anatase TiO_2 powders in an NH_3 (67%)/Ar atmosphere at 600° for 3 h. The nitrogen doping of n-$TiO_{2-x}N_x$ was found to shift the optical absorption and hence photodegredation of methylene blue and gaseous acetaldehyde to the visible region at wavelengths less than 500 nm. Following the observation of the nanostructure activity which we have previously outlined, we have treated TiO_2 nanocolloids (5–20 nm) [24], directly nitriding with alkyl ammonium salts to produce $TiO_{2-x}N_x$ photocatalysts [25] within seconds at room temperature. Further, by adjusting an initial TiO_2 nanoparticle distribution through careful agglomeration and select metal seeding we produce catalytically active $TiO_{2-x}N_x$ constituencies tuned to absorb well into the visible and near infrared regions.

Fig. 3 compares the optical reflectance spectrum for Degussa P25 TiO_2 (reported at an average size of 30 nm), onsetting sharply at ~380 nm, the reflectance spectrum for nitrided, anatase ($TiO_{2-x}N_x$) 3–20 nm nanoparticles, rising sharply at 450 nm, and the corresponding spectrum for

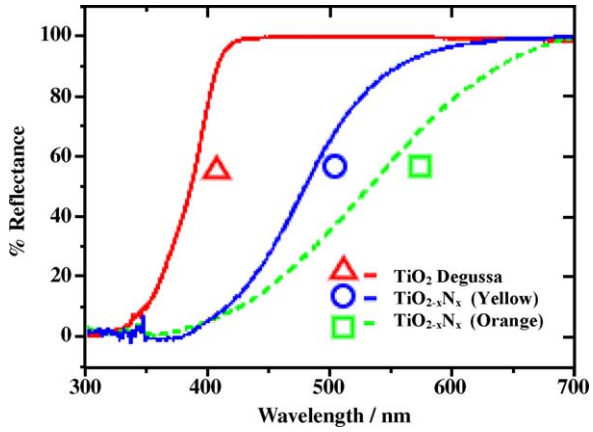

Fig. 3. Reflectance measurements on different TiO_2 samples showing the red-shift effect of nitrogen-doping on the absorption of the nanocrystals.

nitrided ($TiO_{2-x}N_x$) partially agglomerated nanoparticles, rising sharply at 550 nm. We have also introduced Pd into a nitriding amine–TiO_2 mixture. The corresponding reflectance spectrum, obtained as palladium incorporation produces the impregnation of the $TiO_{2-x}N_x$ structure with reduced Pd nanocrystallites [6] and the apparent transformation of some of the $TiO_{2-x}N_x$ anatase structure [6], displays an even broader response extending to considerably longer wavelength, albeit at a notably lower light absorption efficiency as a function of wavelength. In contrast to this nanoparticle activity, no measurable reaction or heat release is observed as either distinct rutile or anatase TiO_2 micropowders are treated directly with an excess of triethylamine.

Photocatalytic activity has been evaluated by measuring the decomposition of methylene blue at 390 and 540 nm, respectively, using a laser producing a 1 kHz pulse train of 120 fs pulses [6,25]. The laser output was used to pump either an optical parametric amplifier to obtain tunable wavelengths in the visible spectrum including 540 nm or a second harmonic generation crystal to produce 390 nm photons. Excitation powers were adjusted using a neutral density filter wheel. Fig. 4 demonstrates the photo-degradation observed at 390 and 540 nm for samples prepared from methylene blue/$TiO_{2-x}N_x$ mixtures in DI water at PH7 [6]. The data for the nitrided samples as well as the palladium treated sample referred to above are consistent with a notable enhanced activity for the $TiO_{2-x}N_x$ constituencies at 390 nm. At 540 nm, all of the nitrided $TiO_{2-x}N_x$ and palladium treated samples still display a notable activity relative to a blank and TiO_2 sample but differences in activity are muted in this less sensitive absorption region [25]. In contrast, at wavelengths below 350 nm, the activity of both the TiO_2 and nitrided samples is comparable. Thus nitrided $TiO_{2-x}N_x$ samples which can be generated in several seconds at room temperature are catalytically active at considerably longer wavelengths than TiO_2. In a preliminary study, the oxynitride has also been used to catalyze the oxidation of ethylene to CO_2 and H_2 [26].

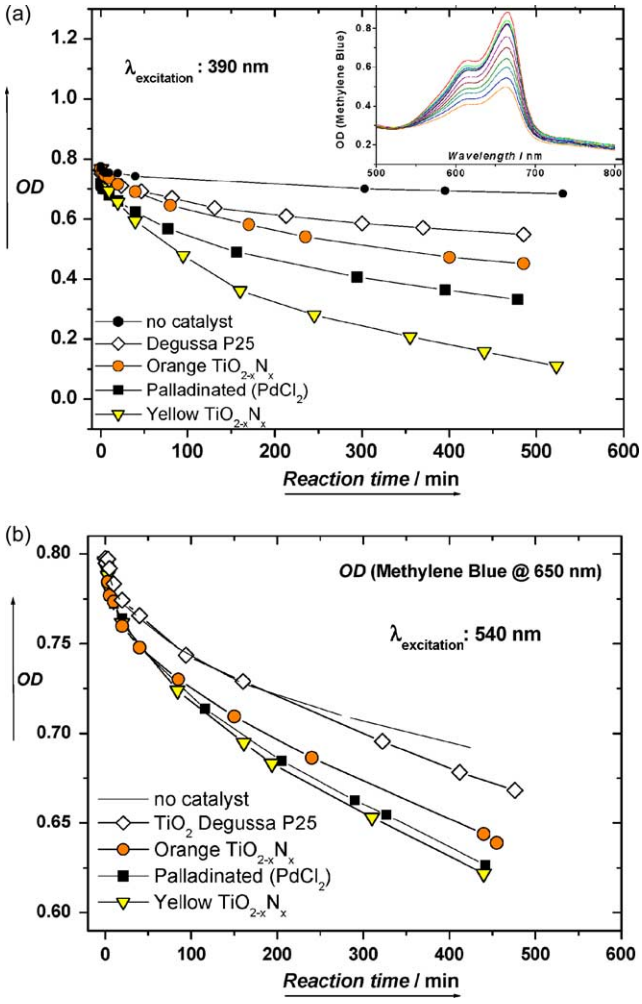

Fig. 4. Comparison of the photocatalytic decomposition of methylene blue after: (a) 390 nm laser excitation, and (b) 540 nm monitored at 650 nm, catalyzed by undoped-TiO_2 (blank test, open diamonds) and nitrogen-doped TiO_2 nanocrystals. The inset in 4(a) shows the photodegradation of methylene blue in water at neutral pH.

The results which we have obtained thus far demonstrate that by forming and adjusting an initial TiO_2 nanoparticle size distribution and mode of nanoparticle treatment, it is possible to tune and extend the absorption of a doped $TiO_{2-x}N_x$ sample well into the visible region. Further, the current study demonstrates that an important modification of a TiO_2 photocatalyst can be made considerably simpler and more efficient by extension to the nanometer regime. The current process can produce submicron agglomerates of a desired visible light absorbing $TiO_{2-x}N_x$ constituency in seconds via a room temperature procedure which otherwise is highly inefficient if not inoperative at the micron scale.

In this paper we have attempted to demonstrate three examples of interesting and surprising chemistry at the nanoscale. We suggest that future experiments will yield comparable and useful surprises.

References

[1] J.L. Gole, J.D. Stout, W.L. Rauch, Z.L. Wang, Appl. Phys. Lett. 76 (2000) 2346.

[2] J.L. Gole, Z.L. Wang, Z.R. Dai, J. Stout, R.P. Gao, M. White, Silica based nanospheres, nanowires, nanosubstrates, nanotubes, and nanofiber arrays, Prog. Colloid Polym. Sci. 281 (2003) 673–685 (Invited Paper).

[3] J.L. Gole, M.G. White, J. Catal. 204 (2001) 249.

[4] J.L. Gole, B.D. Shinall, A.V. Iretskii, M.G. White, W.B. Carter, A.S. Erickson, Tunable surface oxidation states in si/sio$_2$ nanostructures prepared from silicon/silica mixtures and phenol hydroxylation activity, Chem. Phys. Chem. 4 (2003) 1016.

[5] Z.R. Dai, J.L. Gole, Z.L. Wang, J.D. Stout, Tin oxide nanowires, nanoribbons, and nanotubes, J. Phys. Chem. B106 (2001) 1274–1279.

[6] J.L. Gole, C. Burda, et al., Highly efficient formation of visible light tunable $TiO_{2-x}N_x$ photocatalysts and their transformation at the nanoscale, J. Phys. Chem. B108 (2004) 1230–1241.

[7] S.M. Prokes, W.E. Carlos, J.L. Gole, L. Seals, S. Lewis, Mater. Lett. 54 (2002) 85.

[8] C.N. Satterfield, Heterogeneous Catalysis, McGraw-Hill, New York, 1989.

[9] B.C. Gates, Catalytic Chemistry, Wiley, New York, 1992.

[10] The BE's are calibrated against a gold standard (see Ref. [4]) with potential surface charging effects evaluated.

[11] S. Seal, T.L. Barr, S. Krezoski, D. Petring, Appl. Surf. Sci. 173 (3) 339.T. Takami, S. Ishidzuka, Y. Igari, H. Range, I. Kusunoki, Thin Solid Films 89 (2000) 376.

[12] F. Yubero, A. Barranco, J.P. Espinos, A.R. Gonzalez-Elipe, Surf. Sci. 436 (1999) 202.

[13] C.R. Helms, B.E. Deals (Eds.), The Physics and Chemistry of SiO_2 and The Si–SiO_2 Interface, Plenum Press, New York, 1988.

[14] F.G. Bell, L. Ley, Phys. Rev. B 37 (1988) 8383.

[15] J.R. Shallenberger, J. Vac. Sci. Technol. A 14 (1996) 693.

[16] F.J. Grunthaner, P.J. Grunthaner, R.P. Vasquez, B.F. Lewis, J. Maserjian, J. Vac. Sci. Technol. A 16 (1979) 1443.

[17] A thin layer of higher valent silicon, formed due to air exposure, would make only a small contribution to the overall observed oxidation state probed by XPS.

[18] M. Allian, A. Germain, T. Cseri, F. Figueras, Heterogeneous Catalysis and Fine Chemicals III, Elsevier, Amsterdam, 1993.

[19] V.F. Shuvalov, A.P. Moravskii, translated from Doklady Akademii Nauk SSSR, vol. 234, No. 6, pp. 1402–1405, June 1977.G. Centi, S. Perathones, F. Triffiro, J. Phys. Chem. 96 (1992) 2617; K. Fairweg, H. Debellefontaine, Appl. Catal. B Environ. 10 (1996) L229.

[20] M. Suito, N. Kawai, Y. Masuda, Mater. Res. Bull. 10 (1975) 677.

[21] J.L. Gole, Z.L. Wang, Nanoletters I (2001) 449–451.

[22] See for example: (a) A. Fujishima, K. Honda, Nature, 238 (1972) 37;
(b) J.R. Bonton, Sol. Energy, 57 (1996) 37;
(c) S.U.M. Khan, J. Akikusa, J. Phys. Chem. B, 103 (1999) 7184;
(d) S. Licht, et al., J. Phys. Chem., 104 (2000) 8920;
(e) M.R. Hoffman, et al., Chem. Rev., 95 (1995) 69;
(f) D.S. Ollis, H. Al-Ekabi (Eds.), Photocatalytic Purification and Treatment of Water and Air, Elsevier, Amsterdam, 1993.

[23] R. Asahi, T. Morikawa, T. Ohwaki, K. Aoki, Y. Taga, Science 293 (2001) 269.

[24] J.L. Gole, S.M. Prokes, W.E. Carlos, C. She, T. Lian, Surface Modification and Optical Behavior of TiO_2 Nanostructures, Materials Research Society, Proc. Size Depend. Behav. Nanoparticles 239 (2003) 738.

[25] Nitrogen-doped titania nanocrystals for photocatalytic enhancement: spectroscopic evidence for a substitional dopent and comparison to a commercial photocatalyst. (Submitted for publication).

[26] S. Kumar, J.L. Gole, A. Fedorov, Photodegradation of ethylene using visible light responsive surfaces prepared from titania nanoparticle slurries. (Submitted for publication).